X-ray-absorption fine structure study on devitrification of ultrafine amorphous Ni-B alloys

Shiqiang Wei,[1,2,*] Hiroyuki Oyanagi,[2] Zhongrui Li,[1] Xinyi Zhang,[1] Wenhan Liu,[1] Shilong Yin,[3] and Xiaoguang Wang[1]
[1]*National Synchrotron Radiation Laboratory, University of Science and Technology of China, Hefei 230029, People's Republic of China*
[2]*Electrotechnical Laboratory, 1-1-4 Umezono, Tsukuba, Ibaraki 305, Japan*
[3]*Department of Mathematics and Physics, Hohai University, Nanjing 210024, People's Republic of China*
(Received 21 August 2000; revised manuscript received 11 January 2001; published 4 May 2001)

X-ray-absorption fine structure (XAFS), x-ray diffraction, and differential thermal analysis have been combined to investigate the structure of ultrafine amorphous $Ni_{70}B_{30}$ alloy during the crystallization process. The XAFS results demonstrate that a fcc-like nanocrystalline Ni phase with a medium-range order is formed at 573 K where the first exothermic process is observed. We confirmed that the metastable intermediate states consist of the two phases, i.e., nanocrystalline Ni and crystalline Ni_3B alloy. The results support the Riveiro *et al.*'s scenario [J. Magn. Magn. Mater. 188, 153 (1998)] for the devitrification of NiB alloy, in that crystalline phases of Ni_3B and Ni-rich NiB alloy are formed as the intermediate states. Based on the complementary information obtained by the three techniques, we present a simple mechanism of crystallization process for the ultrafine amorphous $Ni_{70}B_{30}$ alloy.

DOI: 10.1103/PhysRevB.63.224201 PACS number(s): 61.10.Ht, 61.43.Dq, 61.46.+w

I. INTRODUCTION

Ultrafine amorphous metal-metalloid NiB and NiP alloys have attracted special attention in view of their unique physical and chemical properties.[1–3] In particular, ultrafine amorphous particles are characterized by small grain size and large static disorder. Hence, they can be easily shaped, suspended in a liquid to make ferrofluid and used for catalysts and magnetic recording materials.[4–6] In order to deeply understand and modify the performances of ultrafine amorphous NiB alloys, it is essential to study both short- and long-range structures of the NiB sample. Hence, a number of studies were focused on investigating their preparation conditions, structures, performances, and stability.[7–13]

Recently, Rojo and co-workers have reported that annealing an amorphous $Ni_{80}B_{20}$ alloy results in an intermediate state that is nanocrystalline with Ni_3B crystallites surrounded by an amorphous pure Ni phase (the amorphous nickel consists of regions with only short-range order, together with regions of nascent crystallinity with a high density of defects), based on the differential scanning calorimeter (DSC), x-ray diffraction (XRD), high-resolution transmission electron microscopy (HRTEM), and magnetic measurements.[14,15] On the contrary, Riveiro and co-workers have explained the broad shoulder superimposed on the XRD peaks of Ni_3B sample as a consequence of overlapping of broad x-ray peaks produced by nanocrystals, using the Rietveld refinement method.[16,17] More recently, the theoretical calculation by Somoza and Gallego has considered that Riveiro's result is a more plausible account of the devitrification of $Ni_{80}B_{20}$ glass.[18] Nevertheless, these conclusions were mainly deduced from XRD, magnetic and electrical resistance measurements. It is very difficult to obtain the local structure from the determination by XRD for a material with a short-range order, since XRD can only give the information on long-range order and lattice strain. Hence, XRD is not suitable to distinguish between an amorphous Ni phase and a nanocrystalline Ni phase with a small grain size in the annealed process of ultrafine amorphous NiB sample.[19]

X-ray-absorption fine structure (XAFS) technique has long been recognized as a powerful tool for determining the local structure of amorphous materials,[20] because of its sensitivity to the short-range order and atomic species surrounding the absorbed atom. Furthermore, one can quantitatively obtain the structural parameters of one element in a complex material by XAFS.[21] In this work, XAFS has been used to investigate the local structure evolutions of ultrafine amorphous NiB alloy during the annealing process. Our XAFS results have revealed that after the first exothermic process, the as-prepared ultrafine amorphous NiB alloy has crystallized to form two metastable crystalline phases of Ni_3B and nanocrystalline Ni with a small grain size at the annealed temperatures of 573 and 623 K. On the other hand, no diffraction peaks corresponding to crystalline Ni can be observed by XRD for these NiB samples.

II. EXPERIMENT

The ultrafine $Ni_{100-x}B_x$ amorphous alloy powder was prepared by adding dropwise an aqueous solution of potassium borohydride (KBH_4, 2 mol/l) into an aqueous mixture solution of nickel acetate [$Ni(CH_3COO)_2 \cdot 4H_2O$, 0.25 mol/l]. The solution was kept in an ice-water bath and vigorously agitated by a magnetic stirrer. The black precipitate was filtered and washed thoroughly with ammonia solution, distilled water, and ethanol, and eventually was soaked in ethanol. Inductively coupled plasma spectrometry showed that the atomic composition of NiB powder is $Ni_{70}B_{30}$. The crystallization process of ultrafine amorphous NiB is described as follows. First, as-prepared NiB powder of 2 g was placed in a pipe furnace, and then flow with a high-purity Ar gas. Second, the sample was slowly elevated to the annealed temperature designed in advance, and was kept at the temperature for 2 h. Finally, the annealed NiB sample was obtained after it was naturally cooled down to room temperature.

The x-ray-absorption spectra at Ni *K*-edge for the as-prepared and annealed $Ni_{70}B_{30}$ samples were measured at the beamline of U7C of National Synchrotron Radiation Labo-

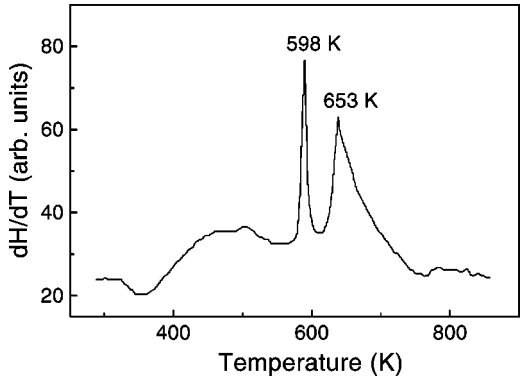

FIG. 1. DTA profile of ultrafine amorphous NiB alloy.

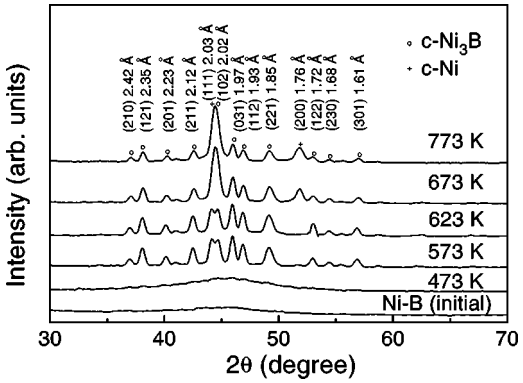

FIG. 2. XRD pattern of ultrafine amorphous NiB alloy annealed at different temperatures.

ratory (NSRL). The storage ring of NSRL was operated at 0.8 GeV with a maximum current of 160 mA. The hard x-ray beam was from a three-pole superconducting Wiggler with a magnetic field intensity of 6 T. The fixed-exit Si(111) flat double crystals were used as monochromator. The XAFS spectra were recorded in a transmission mode with ionization chambers filled with Ar/N_2 at room temperature, using Keithley Model 6517 Electrometer to collect the electron charge directly. XAFS Data were analyzed by USTCXAFS1 data analysis package compiled by Wan and Wei according to the standard procedures.[22,23]

The differential thermal analysis (DTA) profile of ultrafine amorphous $Ni_{70}B_{30}$ alloy powder was performed using CDR-1 differential thermal analysis meter (Shanghai Balance Co.). The samples were heated from room temperature to 873 K with a heating rate of 10 K min^{-1} in a flow of Ar gas of 30 ml min^{-1} at ambient pressure. The XRD patterns of as-prepared and annealed NiB sample were measured on a $Y-4\Phi$ [rotating target diffractometer (Dandong X-ray photometer Co. Ltd.)] using Cu K_α radiation ($\lambda = 1.5418$ Å, 40 kV and 100 mA).

III. RESULTS AND DISCUSSIONS

The DTA profile of ultrafine amorphous $Ni_{70}B_{30}$ alloy in the temperature region between 298 and 873 K is shown in Fig. 1. Two strong exothermic peaks are observed in the DTA profile of ultrafine amorphous NiB alloy. The first peak located at 598 K is sharp while the second peak located at 653 K is broad. Moreover, the area of the second peak is about twice as large as that of the first one. For the annealing temperature beyond 873 K, no new exothermic peak is observed. This indicates that ultrafine amorphous NiB alloy has completely crystallized below 873 K.

Figure 2 exhibits the XRD patterns of the ultrafine amorphous $Ni_{70}B_{30}$ alloy annealed at different temperatures. The as-prepared NiB sample and the one annealed at 473 K keep the amorphous feature, as indicated by a weak broad peak located at $2\theta = 45°$ with the width of 10°. After annealing at 573 K for 2 h, sharp peaks appeared in the XRD curve for the NiB sample. It was found that these diffraction peaks are due to the crystalline Ni_3B and Ni_2B, by comparing with standard ASTM data of nickel, boron, and related compounds. Based on Scherra equation, the average grain size $D_c = 0.89\lambda/(B\cos\theta)$ (here λ, B, and θ are x-ray wave length, width at half height and Bragg angle, respectively), we evaluated that the particle size of crystalline Ni_3B annealed at 573 K is about 30 nm. Using transmission electron microscopy, Deng *et al.*[24] and Li *et al.*[25] have reported that the grain sizes of ultrafine amorphous NiB alloy prepared by chemical reduction method are 50–200 and 100–500 Å, respectively, in good agreement with the present result. With the annealing temperature up to 673 K, a dramatic change of the XRD profile was found for the NiB sample. The diffraction peaks corresponding to crystalline Ni phase has been observed, indicating that crystalline Ni has been formed. Furthermore, the intensity of XRD diffraction peaks of Ni_3B phase evidently decreased. After annealing at 773 K, the diffraction peaks of crystalline Ni phase became dominant for NiB sample. The peak intensities of crystalline Ni_3B in the NiB sample annealed at 773 K were reduced to about half, compared with NiB annealed at 573 K. This result indicates that part of crystalline Ni_3B was segregated into crystalline Ni phase at the temperature of 773 K. However, an appropriate amount of Ni_3B phase still remained.

The radial distribution functions (RDF) of $Ni_{70}B_{30}$ sample after various annealing temperatures, obtained from their $k^3\chi(k)$ by Fourier transform, are displayed in Fig. 3. Only one prominent peak due to the first nearest neighbor of Ni atoms is observed for the as-prepared $Ni_{70}B_{30}$ sample and the

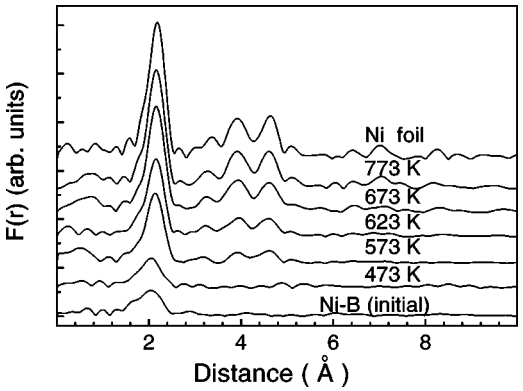

FIG. 3. RDF's of ultrafine amorphous NiB alloy annealed at different temperatures.

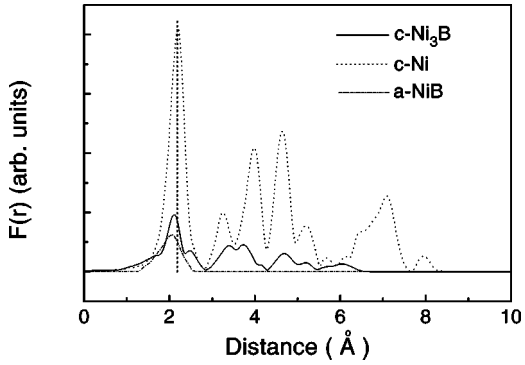

FIG. 4. RDF's of c-Ni, c-Ni_3B, and a-NiB calculated from FEFF7 software package.

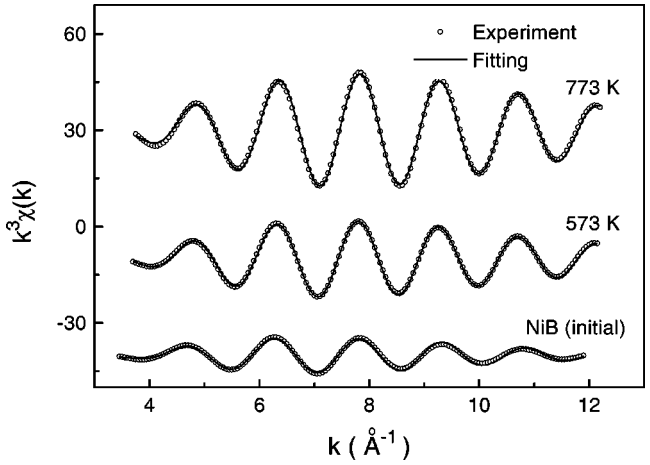

FIG. 5. Fitting results of NiB samples from XAFS data.

one annealed at 473 K. This indicates that there is an amorphous feature in these NiB samples. Crozier,[20] Morrison *et al.*,[26] and we[27] have reported that only one weak peak but no high-distance peak appears for the larger disorder system. After annealing at 573 K, the intensity of the first peak of $Ni_{70}B_{30}$ sample was significantly enhanced, and the second and third nearest-neighbor peaks appeared at the position of 4.0 and 4.6 Å, respectively. The feature of RDF curve of $Ni_{70}B_{30}$ sample annealed at 573 K is the same as that of Ni foil although the magnitude of peak is lower by about 40%. The result implies that the local structure around Ni atoms in the $Ni_{70}B_{30}$ sample annealed at 573 K is similar to that of fcc-structural Ni. In order to analyze the local structures of the as-prepared and annealed $Ni_{70}B_{30}$ samples in detail, the RDF's of crystalline Ni (c-Ni), Ni_3B (c-Ni_3B), and amorphous NiB (a-NiB) were simulated[28] by FEFF7 as shown in Fig. 4. The results show that the intensity of prominent peak of c-Ni_3B is slightly higher than that of a-NiB. However, there is a large difference in the RDF's feature between c-Ni_3B and c-Ni, i.e., the magnitude of the first main peak of c-Ni_3B is much lower, about 25% as that of c-Ni. The reason is that the local coordination environment around Ni atoms is an anisotropic structure for c-Ni_3B,[29] the first nearest neighbor of Ni atoms in c-Ni_3B is surrounded by three B and 11 Ni atoms (one B atom at 2.01 Å, one B atom at 2.05 Å, one B atom at 2.32 Å, one Ni at 2.43 Å, two Ni atoms at 2.47 Å, three Ni at 2.53 Å, three Ni at 2.62 Å, two Ni atoms at 2.72 Å). The distribution of the first nearest-neighbor Ni atoms in a wide region between 2.43 and 2.72 Å, results in a significant decrease of the magnitude of RDF for c-Ni_3B. Wong's result of XAFS measurement has shown that the intensity of the prominent RDF peak of the anisotropic structure c-Ni_2B is about 30% as that of c-Ni,[30] which is in good agreement with our results mentioned above. Therefore, the RDF curve for ultrafine amorphous $Ni_{70}B_{30}$ alloy sample annealed at 573 K cannot be only explained as the formation of c-Ni_3B phase, but also included a metal-like Ni phase although no peaks of metal Ni appear in the XRD pattern. We considered the metastable intermediate state of metal Ni-like phase as a nanocrystalline Ni. For the $Ni_{70}B_{30}$ sample annealed at 773 K, its RDF is almost the same as that of Ni foil. This suggests that at high annealing temperature most of $Ni_{70}B_{30}$ alloy crystallize to form large particles of c-Ni with a long-range order.

The RDF was inversely transformed to isolate the single-shell extended XAFS (EXAFS) contribution. The least-square curve fit technique, based on Marquart's scheme for iterative estimation of nonlinear least-squares parameters via a combination of gradient and Taylor series method[31] was used to fit the inverse transform EXAFS oscillations. For the amorphous NiB alloy, the asymmetric pair distribution function of $G(R)_{asym}$ was assumed as a convolution of Gaussian function P_G and exponential function, P_E.[27,32] The results of curve fit are shown in Fig. 5 and summarized in Table I.

From the DTA and XRD results shown in Figs. 1 and 2, it is concluded that the crystallization process of ultrafine amorphous $Ni_{70}B_{30}$ alloy has two steps. After the first exothermic process at about 598 K, crystalline Ni_3B phase appears in the XRD pattern. However, no diffraction peak indexed to crystalline Ni was found, although one can see that there could be a contribution from the second phase. When the annealing temperature exceeds the second exothermic temperature of 653 K, the intensity of the diffraction peaks of crystalline Ni phase increased, becoming as high as about several times that of crystalline Ni_3B. The result indicates that the stronger and broader exothermic peak at 653 K in the DTA profile is due to the formation of crystalline Ni. This result is nearly identical with that reported by Rojo *et al.*[14] However, Rojo *et al.* have considered that in the first exothermic process, not only crystalline Ni_3B but also an amorphous pure Ni phase with short-range order is formed after the crystallization at 573 K. Their conclusions are further supported by x-ray absorption spectroscopy (XAS)[33] and high-resolution transmission electron microscopy studies.[15] The XAS results have shown that the full width at half maximum (FWHM) of the main absorption peak changed from the initial FWHM of 2.51 eV for the homogeneous amorphous $Ni_{80}B_{20}$ to a value of 2.12 eV for the crystalline mixed phase of Ni and Ni_3B. In the annealing temperature (573 K), an intermediate, partially devitrified state with a FWHM of 2.30 eV was formed, which supports an earlier identification of pure amorphous Ni. From the HRTEM results, Rojo *et al.* explained the Ni intermediate state as an amorphous Ni

TABLE I. The structural parameters of ultrafine amorphous $Ni_{70}B_{30}$ alloy at different annealing temperatures.

Sample	Annealing Temp.	Pair	R_j (Å)	R_0 (Å)	N	σ_T (Å)	σ_S (Å)	δE_0 (eV)
$Ni_{70}B_{30}$	298 K	Ni-Ni	2.75	2.42 ± 0.02	11.0 ± 1.0	0.069	0.33	-0.2
		Ni-B	2.18	2.15 ± 0.02	2.7 ± 0.3	0.046	0.034	-4.7
$Ni_{70}B_{30}$	573 K	Ni-Ni	2.55	2.44 ± 0.02	10.5 ± 1.0	0.060	0.11	-0.9
		Ni-B	2.18	2.15 ± 0.02	2.6 ± 0.3	0.060	0.029	5.0
$Ni_{70}B_{30}$	773 K	Ni-Ni	2.49	2.46 ± 0.02	10.8 ± 1.0	0.070	0.029	1.6
		Ni-B	2.17	2.15 ± 0.02	0.3 ± 0.2	0.056	0.023	-5.0
Ni foil		Ni-Ni	2.49		12.0	0.074		

phase consisting of regions with only a short-range order, together with regions of nascent crystallinity with a high density of defects.

The structural parameters in Table I have shown that the average bond length R_j, coordination number N, thermal disorder σ_T, and the static disorder factor σ_S are 2.75 Å, 11.0 Å, 0.069 Å, and 0.33 Å for the first neighbor of Ni-Ni sub-shell of the as-prepared ultrafine amorphous $Ni_{70}B_{30}$ alloy. After annealing at 573 K, ultrafine amorphous $Ni_{70}B_{30}$ alloy starts to crystallize. Its R_j and σ_S of Ni-Ni subshell decrease notably from 2.75 to 2.55 Å and from 0.33 to 0.11 Å, respectively. The results indicate that the local structure of Ni atoms of $Ni_{70}B_{30}$ sample varies during the crystallization process. The RDF curve shown in Fig. 3 demonstrates that the local structure of $Ni_{70}B_{30}$ sample annealed at 573 K is crystalline with a fcc Ni-like structure. We conclude that a nanocrystalline Ni phase with a small grain size and crystalline Ni_3B alloy are formed for the ultrafine amorphous $Ni_{70}B_{30}$ alloy annealed at 573 K, although no diffraction peaks of crystalline Ni appear in the XRD pattern of this $Ni_{70}B_{30}$ sample. If only the crystalline Ni_3B phase is formed in the first exothermic process, the RDF intensity of the first prominent peak of $Ni_{70}B_{30}$ sample annealed at 573 K should be much lower, like that of crystalline Ni_3B shown in Fig. 4. Hence, our XAFS results support Riveiro's results in that the intermediate state of the NiB sample annealed at 573 K is composed of two crystalline phases, Ni_3B structure with excess Ni and Ni-rich NiB alloy with a lower concentration of B.[17]

From these results mentioned above, the devitrification of ultrafine amorphous $Ni_{70}B_{30}$ alloy into Ni_3B and crystalline Ni seems to occur in a single step. The second DTA exothermic peak (653 K) as shown in Fig. 1 is much larger than those in the Rojo *et al.*'s and Riveiro *et al.*'s experiments.[14,16] It indicates that the second exothermic process in present work is evidently different from those in former results for amorphous NiB alloy. We interpreted that the second exothermic peak is corresponding to two crystallization ways. One is that the grains of nanocrystalline Ni with small size grow into large particles of crystalline Ni. The other is that most of crystalline Ni_3B with small size decomposes into crystalline Ni. It suggests that the decomposition of Ni_3B powder with small size is easier than that of bulk Ni_3B, which has been confirmed by the magnetic measurements.[34] Although the recent interpretations for the devitrification of amorphous NiB alloy seem somewhat controversial, Riveiro, Rojo, and we can have an identical conclusion as long as the intermediate state, noncrystalline Ni phase from Rojo *et al.*'s results,[14,15] were considered as a crystalline Ni phase with large lattice defect. In fact, Rojo *et al.*'s electron diffraction results in that a rather broad ring and an interplanar distance $d=2.03$ Å are corresponding to the Ni-Ni first nearest neighbor distance of metal Ni,[15] have indicated that an intermediate state with Ni-like structure was formed for the amorphous NiB sample annealed at 573 K. Recently, Truskett and Torquato have used parameters of both translational and bond-orientational order for quantifying the disorder in materials,[35] which is suitable to describe the local structures of disorder materials. In our experiment, after annealing at 773 K, the ultrafine amorphous $Ni_{70}B_{30}$ alloy prepared by chemical method[21,36] crystallized into crystalline Ni whose local structure is almost the same as that of fcc Ni. Since the σ_S of Ni-Ni shell of annealed NiB sample decreases to a small value of 0.029 Å, most of NiB alloy has been segregated into crystalline Ni.

Based on DTA, XRD, and XAFS results, we propose a simple mechanism to describe the crystallization of ultrafine amorphous $Ni_{70}B_{30}$ alloy prepared by chemical reduction. The as-prepared NiB sample is composed of a homogeneously amorphous $Ni_{70}B_{30}$ alloy. In the first exothermic process at about 573 K, crystalline Ni_3B, and nanocrystalline Ni with a small grain size are formed. At the higher annealed temperature of 773 K, the metastable NiB intermediate states segregates into large particles of crystalline fcc Ni.

IV. CONCLUSIONS

The XAFS results demonstrated that the local structure of Ni atoms in ultrafine amorphous $Ni_{70}B_{30}$ alloy takes a crystalline fcc-like structure after annealing at 573 K. We find that a nanocrystalline Ni phase with a small grain size is also

formed, although there is no indication of a long-range order. Hence, we conclude that the devitrification of ultrafine amorphous $Ni_{70}B_{30}$ alloy into crystalline Ni_3B and nanocrystalline Ni occurs in the first exothermic process at 573 K. Furthermore, it is likely that the nanocrystalline Ni may form a Ni-rich NiB alloy with a lower B concentration. Our results support Riveiro *et al.*'s conclusion that the intermediate state is composed of two metastable crystalline phases of Ni_3B and Ni-rich NiB alloy. At 773 K, the crystallization of ultrafine amorphous $Ni_{70}B_{30}$ alloy is completed. This implies that most of the crystalline Ni_3B alloy segregate into crystalline Ni and the small nanocrystalline Ni grains grow in size and long-range order at higher annealed temperature.

ACKNOWLEDGMENTS

We would like to thank National Synchrotron Radiation Laboratory and Beijing Synchrotron Radiation Facility for giving us the beam time for XAFS measurement. This work was supported by ''100-people plan'' and ''9·5 programs'' of Chinese Academy of Sciences, and National Natural Science Foundation of China.

*FAX: +86-551-51 4 10 78; Email address: sqwei@ustc.edu.cn

[1] S. Linderoth and S. Morup, J. Appl. Phys. **69**, 5256 (1991).
[2] Y. Chen, Catalysis **44**, 3 (1998).
[3] H. H. Liebermann, *Rapidly Solidified Alloys* (M. Dekker, New York, 1993).
[4] Z. Hu, Y. Fan, and Y. Chen, Appl. Phys. A: Mater. Sci. Process. **A68**, 225 (1999).
[5] L. Ma, W. Huang, J. Yang, and J.F. Deng, J. Phys. IV **7**(C2), 909 (1997).
[6] K. Moorjani, J. D. M. Coey, *Magnetic Glasses* (Elsevier, Amsterdam, 1984), Chap. VIII.
[7] T. Egami and Y. Waseda, J. Non-Cryst. Solids **64**, 113 (1984).
[8] M. Liebs, K. Hummler, and M. Fahnle, Phys. Rev. B **51**, 8664 (1995).
[9] M. Yu and Y. Kakehashi, Phys. Rev. B **49**, 15 723 (1994).
[10] J. Saida, A. Inoue, and T. Masumoto, Mater. Sci. Eng., A **133**, 771 (1991).
[11] H.X. Li, H.Y. Chen, S.Z. Dong, J.S. Yang, and J.F. Deng, Appl. Surf. Sci. **125**, 115 (1998).
[12] Ch. Hausleitner and J. Hafner, Phys. Rev. B **47**, 5689 (1993).
[13] A.M. Bratkovsky and A.V. Smirnov, J. Phys.: Condens. Matter **3**, 5153 (1991).
[14] J.M. Rojo, A. Hernando, M.E. Ghannami, A. Garcia-Escorial, M.A. Gonzalez, R. Garcia-Martinez, and L. Ricciarelli, Phys. Rev. Lett. **76**, 4833 (1996).
[15] C. Ballesteros, A. Zern, A. Garcia-Escorial, A. Hernando, and J.M. Rojo, Phys. Rev. B **58**, 89 (1998).
[16] J.M. Riveiro, P. Muniz, J.P. Andres, and M.A. Lopez de la Torre, J. Magn. Magn. Mater. **188**, 153 (1998).
[17] J.M. Riveiro and P. Muniz, Phys. Rev. B **58**, 11 093 (1998).
[18] J.A. Somoza and L.J. Gallego, Phys. Rev. B **61**, 3177 (2000).
[19] E. D. Crozier, J. J. Rehr, and R. Ingalls, in *X-ray Absorption, Principles, Applications, Techniques of EXAFS, SEXAFS and XANES*, edited by D. C. Koningsberger and R. Prins (Wiley, New York, 1988), p. 373.
[20] E.D. Crozier, Physica B **208,209**, 330 (1995).
[21] B.R. Shen, S.Q. Wei, K.N. Fan, and J.F. Deng, Appl. Phys. A: Mater. Sci. Process. **A65**, 295 (1997).
[22] X. H. Wan, S. Q. Wei, *USTCXAFS Software Package* (1999).
[23] D. E. Sayers and B. A. Bunker, in *X-ray Absorption, Principles, Applications, Techniques of EXAFS, SEXAFS and XANES* (Ref. 19), p. 211.
[24] J.F. Deng, J. Yang, S.S. Sheng, H.R. Chen, and G.X. Xiong, J. Catal. **150**, 434 (1994).
[25] T.X. Li, X.F. Zhang, H.Q. Li, C.D. Jin, Y.L. Jiang, J.T. Cui, and D.Q. Wang, Chin. J. Catal. **16**, 299 (1995).
[26] T.I. Morrison, C.L. Foiles, D.M. Pease, and N.J. Zaluzec, Phys. Rev. B **36**, 3739 (1987).
[27] S.Q. Wei, H. Oyanagi, W.H. Liu, T.D. Hu, S.L. Yin, and G.Z. Bian, J. Non-Cryst. Solids **275**, 160 (2000).
[28] J.J. Rehr, S.I. Zabinsky, and R.C. Albers, Phys. Rev. Lett. **69**, 3397 (1992).
[29] B. Aronsson, Acta Chem. Scand. **9**, 137 (1955).
[30] J. Wong and H.H. Liebermann, Phys. Rev. B **29**, 651 (1984).
[31] D.W. Marquardt, J. Soc. Ind. Appl. Math. **11**, 431 (1963).
[32] L.W. Wu, S.Q. Wei, B. Wang, and W.H. Liu, J. Phys.: Condens. Matter **9**, 3521 (1997).
[33] A. Gutierrez, M.F. Lopez, A. Hernando, and J.M. Rojo, Phys. Rev. B **56**, 5039 (1997).
[34] S. Q. Wei, Z. R. Li, X. Y. Zhang, and W. H. Liu (unpublished).
[35] T.M. Truskett, S. Torquato, and P.G. Debenedetti, Phys. Rev. E **62**, 993 (2000).
[36] S. Q. Wei, Z. R. Li, S. L. Yin, X. Y. Zhang, W. H. Liu, and X. G. Wang, J. Synchrotron Radiat. **8**, 566 (2001).